Numerical Solution of the Navier-Stokes Equations for a Three-Dimensional Corner

J. S. Shang* and W. L. Hankey†
Air Force Flight Dynamics Laboratory, Wright-Patterson Air Force Base, Ohio

A three-dimensional, time dependent Navier-Stokes code employing MacCormack's finite-difference scheme has been developed. Successful comparisons were performed for analytic solutions first to validate the numerical procedure. The strong inviscid-viscous interacting flowfield for a three-dimensional compression corner at a Mach number of 12.5 and a Reynolds number of 1.21×10^6 was then computed and compared with experiment. The computed result nearly duplicated the experimental observations, including wall pressure, heat transfer, oil flow streamline pattern, and impact pressure flowfield survey. The numerical result not only verified the experimental finding of an extensive penetrating inviscid stream (inviscid finger) in the corner region as the source of the extremely high local rate of heat transfer, but also revealed an embedded crossflow supersonic region in the viscous vortex. The present result tends to substantiate the separation criterion established by the limiting line theory, in which the separation line is defined as an envelope of limiting streamlines. This investigation demonstrated that numerical methods may be used to determine the general features of complex three-dimensional flows.

Nomenclature

c	= speed of sound
C_v	= specific heat at constant volume
Def	= deformation tensor
e	= specific internal energy, $C_vT+\Sigma u_m^2/2$
F,G,H	= vector fluxes, Eq. (3a)
i,j,k	= indexes of the grid-point system
$\bar{\bar{I}}$	= unit identity matrix
k	= molecular heat conductivity
k_1,k_2	= exponents in the stretched coordinates y, z, respectively
M	= Mach number
p	= static pressure
$\dot{q}$	= rate of heat transfer
Re	= Reynolds number
t	= time
T	= static temperature
$\bar{u}$	= velocity vector
$\bar{U}$	= vector of the dependent variable, Eq. (3a)
u,v,w	= velocity components in Cartesian frame
X_m	= x,y,z Cartesian coordinates
$\tilde{x}_L,\tilde{y}_L,\tilde{z}_L$	= length scales in conical coordinates
α	= stream surface deflection angle
α_d	= coefficient in pressure damping terms, Eq. (4b)
γ	= limiting stream deflection angle at the plate surface
ξ,η,ζ	= transformed coordinate system, Eq. (2)
$\xi_{x_m},\eta_{x_m},\zeta_{x_m}$	= coordinate transformation derivatives
θw	= wedge angle with respect to freestream
θ,ϕ	= angular bases in spherical coordinate system
μ	= molecular viscosity coefficient
λ	= bulk viscosity coefficient
Φ	= work done by viscous stress
ρ	= density
Σ	= summation
$\bar{\bar{\tau}}$	= tensor stress
$\bar{\bar{\tau}}'$	= viscous stress $\bar{\bar{\tau}}'=\bar{\bar{\tau}}+p\bar{\bar{I}}$

Subscripts

∞	= property evaluated at the freestream condition
w	= property evaluated at solid surfaces
m	= coordinate indexes 1,2,3
0	= stagnation condition

Superscripts

$-$	= denotes vector
$=$	= denotes tensor
$*$	= variables in corrector operation
n	= denotes time level

Received Nov. 9, 1976; presented as Paper 77-169 at the AIAA 15th Aerospace Sciences Meeting, Los Angeles, Calif., Jan. 24-26, 1977; revision received June 15, 1977.

Index categories: Supersonic and Hypersonic Flow; Viscous Nonboundary-Layer Flows.

*Aerospace Engineer. Member AIAA.

†Senior Scientist. Member AIAA.

I. Introduction

FOR two-dimensional viscous-inviscid interactions with flow separation, the mathematical structure has been developed by means of an elegant asymptotic expansion scheme.[1] However, no development of a proper mathematical description of the nature or structure of the three-dimensional problem has been documented. Experimental research in three-dimensional flowfields generally has provided only a partial understanding of the observations. Then, it is logical to consider a numerical analysis for a typical three-dimensional interacting flow, including flow separation, in an attempt to provide some additional information on the essential features of this flowfield. In spite of the rapid advancement in numerical analysis in aerodynamics, only a few two-dimensional numerical solutions of the Navier-Stokes equations have been obtained and even fewer three-dimensional numerical solutions documented.[2]

On the selection of a typical three-dimensional interaction with flow separation, for the present numerical analysis many practical aspects had to be considered. The three-dimensional corner flow problem meets many of these requirements. First, this configuration is common to many engineering problems; i.e., inlets, the fuselage-wing junction and the intersection of several control surfaces.[3] For sufficiently large deflections of the surface with respect to the freestream, strong shock waves result which induce flow separation. Secondly, extremely high rates of heat transfer occur in the corner region which can cause catastrophic structural failure; however, mechanisms of the hot spot have not been identified. Hence the un-

derstanding of the flowfield becomes necessary before any remedy can be implemented successfully.

For the three-dimensional compression corner problem, inviscid calculations have been obtained by Kutler,[4] and Shankar and Anderson.[5] Since the viscous effect was ignored, an important aspect of the inviscid-viscous interaction associated with the corner region remained unresolved. Asymptotic viscous solutions also were obtained by Weinberg and Rubin[6] and Ghia and Davis[7] for flow bounded by two intersecting flat plates. The primary interest of their work is to determine the first higher-order potential flow in the corner as well as the resulting secondary crossflow in the boundary layer. The strong inviscid and viscous interaction is also explicitly excluded.

The present analysis attempts to demonstrate the feasibility of numerically solving a three-dimensional compression corner flow accentuated by a strong inviscid-viscous interaction. The full Navier-Stokes equations were utilized in order to describe fully the basic interaction with flow separation. An explicit numerical scheme was selected over an implicit method[8] due to recent successes in computing flowfields containing shock waves.[9-11] The three-dimensional computation was accomplished for an axial compression corner generated by a 15 deg wedge and flat plate at a hypersonic Mach number of 12.5. The corresponding unit Reynolds number based upon freestream properties was about 10^6/ft. Comparisons were performed with experimental[12] surface pressure measurements, pitot pressure data, and surface oil film flow patterns. The entire flowfield structure will be presented in the form of density contours, crossflow velocity vector diagrams, surface shear and heat-transfer distributions. Finally, the three-dimensional flow separation phenomenon will be discussed.

Governing Equations

The governing equations for the present analysis are the unsteady compressible three-dimensional Navier-Stokes equations. The time dependency of the governing equations permits the solutions to progress naturally from an arbitrary initial guess to an asymptotic steady state.[13]

$$\frac{\partial \rho}{\partial t} + \nabla \cdot (\rho \bar{u}) = 0 \tag{1a}$$

$$\frac{\partial \rho u}{\partial t} + \nabla \cdot (\rho \bar{u} u - \bar{\bar{\tau}}) = 0 \tag{1b}$$

$$\frac{\partial \rho e}{\partial t} + \nabla \cdot (\rho e \bar{u} - \bar{u} \cdot \bar{\bar{\tau}} + \dot{\bar{q}}) = 0 \tag{1c}$$

The system of equations is in perfect divergent form, with the dependent variables of the system of equations identified as ρ, $\rho\bar{u}$, and ρe. This grouping of the variables constitutes the so-called conservative form. The equations of state, Sutherland's viscosity law, and assigned Prandtl number (0.73) formally close the system of equations. The associated boundary conditions for the problems considered will be delineated in a subsequent section.

A major difficulty encountered in analyzing practical three-dimensional aerodynamic problems is the accommodation of complicated body configurations. A general coordinate transformation was successfully demonstrated by Knight and Hankey[14] in their investigations of a two-dimensional supersonic diffuser. In the present analysis, the coordinate transformation is introduced as

$$\xi = \xi(x) \tag{2a}$$

$$\eta = \eta(x,y,z) \tag{2b}$$

$$\zeta = \zeta(x,y,z) \tag{2c}$$

Transformation of the independent variables is sufficiently flexible to treat a large category of aerodynamic configurations and yet is not overly complex and does not require excessive computer storage. The dependent variables, however, remain unaltered.

The governing equations in the transformed space are in the following form:

$$\frac{\partial \bar{U}}{\partial t} + \xi_x \frac{\partial \bar{F}}{\partial \xi} + \sum_m \eta_{x_m} \frac{\partial \bar{G}_m}{\partial \eta} + \sum_m \zeta_{x_m} \frac{\partial \bar{H}_m}{\partial \zeta} = 0 \tag{3a}$$

where $m = 1, 2, 3$; the ξ_{x_m}, η_{x_m}, and ζ_{x_m} denote the first-order partial derivatives of the transformed independent variables (ξ,η,ζ) with respect to the coordinates (x,y,z) of the Cartesian system. The vector fluxes F, G_m, and, H_m are defined as follows:

$$F = G_1 = H_1 = \begin{bmatrix} \rho u \\ \rho u u - \tau_{xx} \\ \rho u v - \tau_{xy} \\ \rho u w - \tau_{xz} \\ \rho e u + \dot{q}_x - \Phi_x \end{bmatrix} \tag{3b}$$

$$G_2 = H_2 = \begin{bmatrix} \rho v \\ \rho v u - \tau_{yx} \\ \rho v v - \tau_{yy} \\ \rho v w - \tau_{yz} \\ \rho e v + \dot{q}_y - \Phi_y \end{bmatrix} \tag{3c}$$

$$G_3 = H_3 = \begin{bmatrix} \rho w \\ \rho w u - \tau_{zx} \\ \rho w v - \tau_{zy} \\ \rho w w - \tau_{zz} \\ \rho e w + \dot{q}_z - \Phi_z \end{bmatrix} \tag{3d}$$

where the heat flux is defined as $\dot{q} = \kappa \nabla T$, and the viscous dissipation function Φ is given as $\bar{\Phi} = \bar{u} \cdot \bar{\bar{\tau}}'$. The complete stress components contained in Eqs. (3) can be obtained from the stress tensor

$$\bar{\bar{\tau}}' = -p\bar{\bar{I}} + \lambda(\nabla \cdot \bar{u})\bar{\bar{I}} + \mu \text{ Def } \bar{u} \tag{3e}$$

and the chain rule of differentiation.

Numerical Procedure

The system of equations is solved by a two-step predictor and corrector scheme originated by MacCormack.[15] The stress and heat flux terms in the flux vector F, G, and H are approximated by a central, forward, and backward differencing scheme in such a fashion that after a complete cycle of the predictor and corrector operations the second derivations are effectively approximated by a central differencing scheme. In essence, the differencing operations aligned with a transformed coordinate are represented by a combination of backward and forward differencing schemes. The derivatives which do not align with the transformed coordinates are approximated by a central differencing scheme.

Equation (3a) is split into three groups of operators, each aligned with a transformed coordinate. Therefore, an alternating direction procedure can be implemented easily. Time splitting (A.D.E) is an option in the present version of the code; however, it was not utilized in this investigation.

The present numerical scheme is a generalization of MacCormack's numerical method[15] for two-dimensional Navier-Stokes equations into the three-dimensional domain. The numerical scheme is second-order accurate in space and time.[9,15] Although to date no completely satisfactory stability analysis has been performed for the finite-difference form of the Navier-Stokes equations,[9] the Courant-Friedrich-Lewy (CFL) conditions for the inviscid domain serves as a useful guide.[16]

$$\Delta t_{\mathrm{CFL}} \leq \min \left[\frac{|u|}{\Delta x} + \frac{|v|}{\Delta y} + \frac{|w|}{\Delta z} + c\sqrt{\frac{1}{\Delta x^2} + \frac{1}{\Delta y^2} + \frac{1}{\Delta z^2}} \right]^{-1} \tag{4a}$$

For the viscous dominant region, an empirical formula suggested by Tannehill et al.[17] or the results of MacCormack's time splitting procedure seem to be adequate. The lack of a rigorous criterion in the allowable time step (stability analysis) for the present investigation is the primary reason that a meaningful optimization of the present numerical code was not attempted. Successful solutions were obtained, however, by using a conservative fraction of the CFL time step.

Flows containing strong shock waves often cause numerical oscillations. The large trunction errors in the early transitory stage of the computations also may cause divergence of the developing numerical solution. Two numerical smoothing schemes were incorporated into the present numerical procedure. The fourth-order pressure damping suggested by MacCormack[9] was adopted with modification. Instead of using a rigorous transformation of the second-order derivatives of pressure into the transformed space, the second-order derivations of pressure are approximated by the derivatives with respect to the transformed independent variable (ξ,η,ζ). The net result is an artificial viscosity-like term of the form

$$-\alpha_d \Delta t \Delta \xi_m^3 \frac{\partial}{\partial \xi_m}\left[\frac{u_m + c}{4p}\frac{\partial^2 p}{\partial \xi_m^2}\right]\frac{\partial U}{\partial \xi_m} \qquad m=1,2,3 \tag{4b}$$

added to the difference equations. The result is identical to MacCormack's expression if the Cartesian coordinate system were used. Tannehill et al.[17] also modified the fourth-order damping terms in a similar manner, except they replaced the second-order derivative of pressure by the second-order derivative of density. This damping term is only of significant magnitude in regions of pressure oscillation where the trunction error is already degrading the computation. Additional normal stress damping due to McRae[18] designed to counteract the abnormal transitory behavior also was included. The additional stress damping was used only for the relatively coarse grid-point system and was completely removed after a very short duration for the initial phase of the iteration process. These damping terms are so designed to be only effective in the inviscid field and hence do not appreciably change boundary-layer behavior or modify the Reynolds number.

Boundary Conditions and Coordinate Systems

The axial corner was formed by the orthogonal intersection of a 15-deg wedge and a flat plate (Fig. 1). The freestream Mach number was 12.5, and the Reynolds number based upon the axial length was 1.21×10^6. Laminar flow was found to exist throughout for the stated conditions. The inviscid computations[4,5] of the flowfield around the compression corner revealed a rather complicated intersecting shock wave system with a slip surface. The experimental investigation[12] indicated similar results; in addition the surface oil film flow pattern showed extensive separated flow regions. This evidence is obviously a consequence of the strong inviscid-viscous interaction. A feature that stands out in the experimental investigations is the fact that the shock wave structure and surface pressure measurements exhibit an approximate conical characteristic.[12] In other words, the inviscid dominant portion of the flowfield is nearly invariant with respect to a generating radius vector from the apex of the corner, regardless of the different scaling of the growth of the viscous region. This outstanding feature of the flowfield has led to the adoption of the conical coordinate system for the present investigation.

The coordinate system utilized is given as follows:

$$\xi = x/x_L \tag{5a}$$

$$\eta = (1/k_1)\ell n[1 + (e^{k_1} - 1)(y/x)/\tilde{y}_L] \tag{5b}$$

$$\zeta = (1/k_2)\ell n[1 + (e^{k_2} - 1)\{(z/x) - \tan\theta_w\}/\tilde{z}_L] \tag{5c}$$

where k_1 and k_2 were uniquely determined by the minimum step size and number of grid points. In order to achieve the appropriate grid spacing to resolve the significant features of this flowfield, the conical coordinates normal to the surfaces were stretched exponentially [Eqs. (5b) and (5c)] to yield a unit cell Reynolds number near two. This insures that the boundary layer contains about 10 points. The coordinate transformation derivatives are easily obtainable from Eqs. (5a-5c) and therefore will not be presented here.

In the transformed space, the domain of the independent variables are defined to be

$$0.125 < \xi < 1.0 \tag{5d}$$

$$0 < \eta < 1.0 \tag{5e}$$

$$0 < \zeta < 1.0 \tag{5f}$$

The grid-point spacings are uniformly distributed in each respective coordinate; thus, the transformed space is represented by a cube. The origin of the coordinate system is also located in the freestream to avoid the singular behavior at $x=0$. The computational domain has maximum dimensions of 12.5 in. $\times$ 3.4 in. $\times$ 12.5 in. defined by $X_L = 1.166$, $Y_L = 0.24$, and $Z_L = 0.7321$ (Fig. 1).

The initial and boundary conditions for the compression corner flow are summarized as follows:

Upstream and initial conditions were prescribed by the values of the unperturbed freestream.

Initial condition:

$$\bar{U}(0,\xi,\eta,\zeta) = \bar{U}_\infty \tag{5g}$$

Upstream condition:

$$\bar{U}(t,\ 0.125,\ \eta,\zeta) = \bar{U}_\infty \tag{5h}$$

The boundary conditions on the solid contour are the no-slip conditions for the velocity components and a constant surface

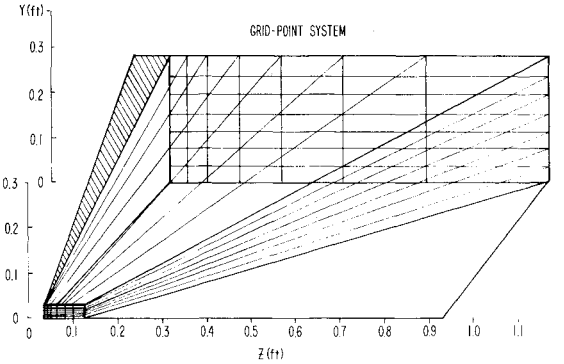

Fig. 1 Three-dimensional compression corner coordinate system.

temperature (660°R). The latter is intended to duplicate the experimental wall temperature:

$$u=v=w=0, \text{ at } \eta=0, \text{ or } \zeta=0 \tag{5i}$$

$$Tw=660°\text{R}, \text{ at } \eta=0, \text{ or } \zeta=0 \tag{5j}$$

The boundary condition for pressure at the solid surfaces is obtained by satisfying the momentum equations at the surface. The derivatives contained in the momentum equations were approximated by one-sided differencing. Once the value of the surface pressure is determined, the value of density is obtained through the equation of state. However, since the shear gradients were found to be small, the following approximation was optional for the present analysis:

$$\frac{\partial p}{\partial \eta}=0, \qquad \text{at } \eta=0 \tag{5k}$$

$$\frac{\partial p}{\partial \zeta}=0, \qquad \text{at } \zeta=0 \tag{5l}$$

For the far-field boundary conditions, gradients are set equal to zero in all coordinate directions. $\partial U/\partial \eta=0$ and $\partial U/\partial \zeta=0$ reflect the fact the flow returns to two-dimensional flow far away from the corner. The downstream condition indeed is a consistent approximation; $\partial U/\partial \xi=0$ implying conical similarity at the far downstream boundary.

Discussion of Results

For the present analysis, all but the finest mesh computations were performed on a CDC 6600 digital computer. The calculation of the finest mesh system was performed on the CDC 7600 computer of NASA Ames Research Center. The rate of data processing was 0.00398 sec per grid point for each time step. The evolution of the numerical solution was monitored until consecutive results indicated no significant change during certain fractions of time that a fluid particle requires to travel along the corner. The solution then was considered to be the asymptotic steady-state solution. The total computing time for the finest mesh system was 10 hr on a CDC 7600 computer. The need for improving numerical efficiency becomes obvious.

Since experiments indicated that the variation of flow in the streamwise direction is relatively mild in comparison with the "crossflow" plane, adequate numerical resolution probably can be achieved by only a few stations in the streamwise direction. Taking advantage of this salient characteristic, three grid-point systems were selected; (8, 12, 20), (8, 20, 28), and (8, 32, 36). A truncation analysis was conducted by comparing the numerical results of the three-grid-point systems with experimental measurements.[12,19] In physical space the computational domain was the frustrum of a rectangular pyramid (Fig. 1). The dimensions of the cross section enlarge linearly in the direction of the freestream. The grid-point spacing was smallest at the leading edge in order to resolve adequately the rapidly developing flowfield.

Numerical results are presented in two groups. In the first portion we are seeking confirmation of the numerical results by comparing with experimental measurements. A truncation analysis also is presented and compared with data. The second group of the presentation is intended to interpret the flowfield structure in terms of the numerical results.

In Fig. 2, the experimental surface pressure measurements[12,19] on the plate along with the numerical results are presented. The agreement between the measurements and calculation is excellent. In general, the numerical results either with the coarser mesh systems or the finer mesh systems are confined within the data scattering. The trough-like pressure variation outward from the wedge-induced shock, identified by Korkegi[3] as the indication of the embedded secondary flow separation, was predicted by the numerical results. The fine mesh calculation, however, revealed a much better definition.

In Fig. 3, the pitot pressure data of Cooper and Hankey[19] is presented in isobar form. The intersection of the vertical wedge and horizontal plate surface is defined as the origin of the graph. The data were collected at a streamwise distance of 12.5 in. from the leading edge. A total of 1355 data points were evaluated to produce the impact pressure contour. The intricate shock structure was revealed in the form of concentrated isobars; the shock wave surface induced by the wedge is clearly defined as a band of concentrated isobars to the right side of the viscous layer on the vertical wedge surface. The coalesced shock waves due to the growth of the boundary layer on the plate are also obviously identified as the upper band of concentrated isobars. Beneath the coalesced shock waves, the outer edge of the boundary layer developed on the plate is also indicated. The oscillatory contour lines on the right-hand side of the graph are a consequence of sparse experimental data in that region. In the inner corner, the two shock-wave systems intersect and produce a series of triple points.[19] The interacting shock waves deflect inward and toward the corner, as the local Mach number further decreases deeply within the viscous region on the plate, and a gradual compression is indicated. The boundary-layer development on the wedge surface is reflected in a condensed band of isobars (inner vertical band). The boundary layer on the plate is subjected to a much lesser external pressure than on the wedge, and thus the thickness of the boundary layer is greater, as one would expect.

Figure 4 represents the typical numerical simulation of the pitot pressure contours (560 points). The contour was generated at identical contour levels as that for the experimental data; i.e., increments at 10 mm Hg. It is obvious that the numerical results duplicated all of the essential features observed in the experiment. However, the numerical result exhibits a certain amount of shock wave smearing as anticipated. The computation also underpredicts the thickness of the viscous dominant region; and, as a consequence, the

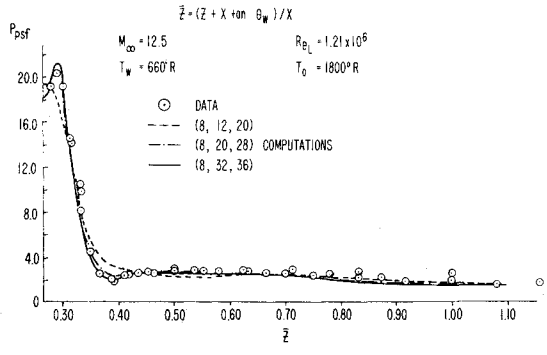

Fig. 2 Comparison of surface pressure distribution for different mesh sizes.

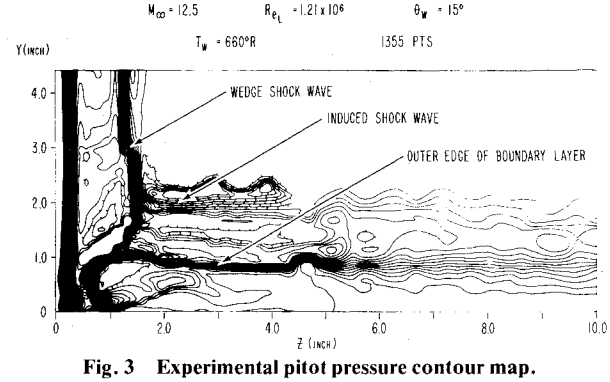

Fig. 3 Experimental pitot pressure contour map.

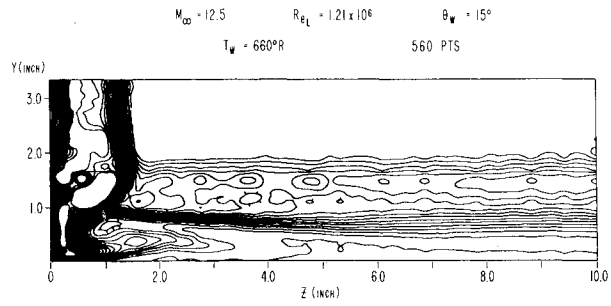

Fig. 4 Computed pitot pressure contour map.

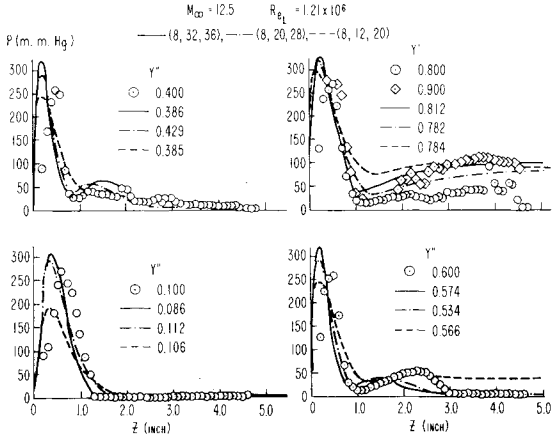

Fig. 5 Comparison of pitot pressure distribution $0 < y < 0.8$ in.

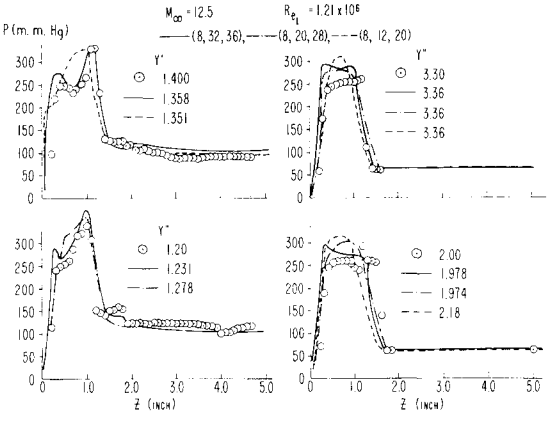

Fig. 6 Comparison of pitot pressure distributions 1 in. $< y < 3.4$ in.

shock wave system is displaced slightly inward to the surface. This particular shortcoming, we feel in principle, can be remedied by increasing the numerical resolution in the axial direction (ξ). In all, the agreement between the experimental data and calculation is considered to be remarkable for the limited number of grid points.

In Figs. 5 and 6, the pitot pressure data[12,19] and numerical results are compared in a different format. In these figures, a comparison of pitot pressure distributions is presented for a fixed location y above the plate surface. The major deficiency as pointed out earlier was in the prediction of the thickness of the viscous region. Also, the predicted shock-wave locations are displaced slightly toward the surfaces. The prediction by the fine mesh system agrees much better with the data than the results by the coarser mesh system. Both numerical results, however, yield nearly identical behavior as that of experimental measurements.

The surface oil film flow of the experimental measurement is presented in Fig. 7. According to the limiting streamline

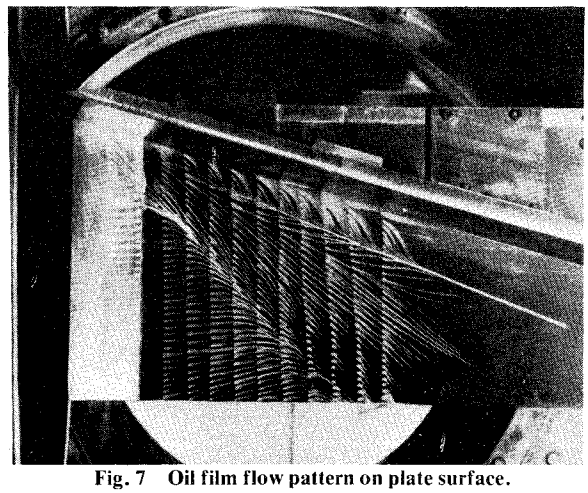

Fig. 7 Oil film flow pattern on plate surface.

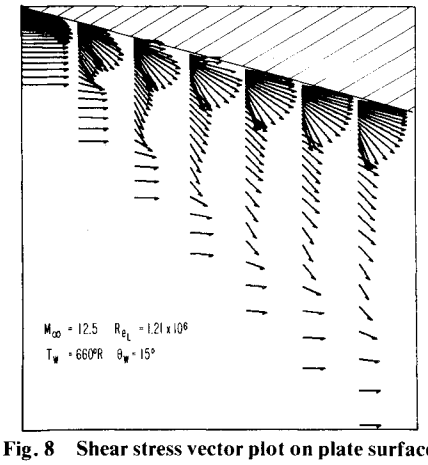

Fig. 8 Shear stress vector plot on plate surface.

concept, the separation line may be defined as the locus of the intersection of consecutive elements of a family of limiting streamlines[20-23] (i.e., envelope). The separation streamline for a three-dimensional flow will be indicated by a convergence of surface streamlines, or oil streaks for experimental observation.[3,19,24] A general definition is still controversial[21,23,24]; however, we consider the main characteristics of a line of separation as the tangential convergence of the surface streamline onto one single line inclusively. From Fig. 7 one can identify two sets of convergent oil streaks and divergent streaks. Therefore, there are two separations and reattachments in compliance with this aforementioned criterion.

The calculated surface force in vector form is presented in Fig. 8. The magnitude of the resultant force differs by an order of magnitude from the corner regions and decays rapidly toward the outer region. The total force also decays gradually from the leading edge to the trailing regions by a factor of 2.3. In order to prevent overlapping the vectors, the cube root of shear stress was plotted. In Fig. 7 the convergent lines are easily detected. On the surface two convergent rays originating from the corner are presented. The outer convergent line is at a deflection angle of 44 deg with respect to the freestream, while the inner convergent line forms a deflection angle of about 22 deg. These lines vary only slightly from the leading edge as they develop downstream. The divergent lines are more difficult to detect than the convergent lines, but the innermost divergent line can be identified to be deflected about 17 deg from the freestream, while the outer divergent line is at 27 deg as reflected in the experimental oil film photograph. The numerical result of the surface forces (Fig. 8) duplicates the outer separation and[12,19] inner reattachment line but fails to capture the secondary vortex.

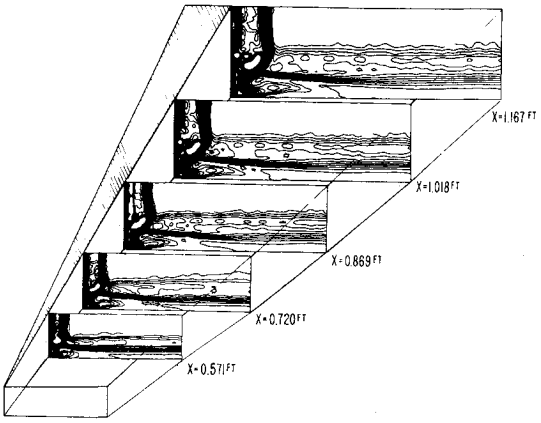

Fig. 9 Density contour map of the three-dimensional flowfield.

In essence, the numerical results reproduce the outstanding features of the experimental observation.[12,19] The qualitative and quantitative agreement between the experiment and calculations confirms that the present numerical analysis correctly predicted the physical phenomenon. The affinity between numerical results by different grid spacing also verifies that the present analysis has a credible numerical resolution.

Based upon the numerical results, we will attempt to derive an understanding of the rather complex flowfield structure. First, one recognizes that the entire flowfield structure is primarily conical,[12,19,25] namely, the shock-wave formation is nearly invariant along a generating ray emanating from the apex of the corner. The viscous dominated region plays a relatively passive role in determining the enveloping shock-wave system for the corner configuration. However, the viscous dominated region produces the most intricate fluid mechanics phenomena. In Fig. 9, the density contour of the entire three-dimensional flowfield is presented in which the shock waves and viscous dominant regions are represented by highly concentrated constant density lines. Indeed, the shock-wave structure is nearly conical. In this figure, one can also clearly identify the induced and coalesced shock waves due to the growth of boundary layer on the plate (upper, horizontal band of density contours). The high-density gradient zone beneath the induced shock waves signifies the outer portion of a hypersonic boundary layer (lower, horizontal band of density contours). The thickness of boundary layer changes gradually from the corner outward and eventually attains a constant height from the plate. This behavior signifies the asymptotic approach of a two-dimensional flow far from the corner.

The shock wave generated by the wedge is clearly observable as well as the highly compressed boundary layer on the wedge surface (vertical band of density contours). A drastic flowfield structure change occurs below the intersection of the wedge shock and the induced shock waves. The phenomenon was completely described by the triple point analysis given by Cooper and Hankey in their evaluation of the experimental data.[19] At the intersection of the shock waves, an embedded shock wave is formed to satisfy pressure continuity and flow direction requirements across the slip surface. Once the triple point is located, the adjacent flowfield properties are completely determined.[19] Again, the numerical result substantiates their observation that, for this asymmetric corner configuration, only one triple point exists. However, for a symmetrical corner generating by two wedges, a set of two triple points is obtained.[4,5] The reason for this difference is that inboard of the wedge shock the crossflow Mach number is subsonic, thereby permitting the shock to curve away from the triple point to attain the required boundary condition. The present numerical result verifies this contention.

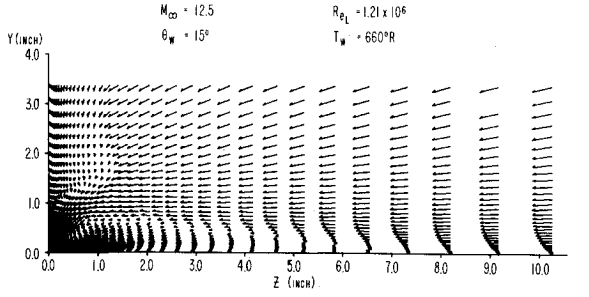

Fig. 10 Crossflow vector velocity plot in conical coordinates ($x = 12$ in.).

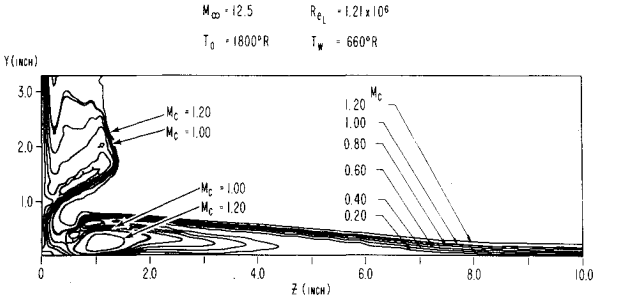

Fig. 11 Crossflow Mach number contour.

Since the surface oil flow patterns and the shock-wave system reflect a nearly conical flow structure, the velocity components in a spherical coordinate system are most suitable in delineating the three-dimensional flowfield. In Fig. 10, the conical crossflow velocity component is projected on to the y-z plane. The velocity is oriented at an angle of $\gamma - \phi$ on that plane: where $\tan\gamma = u_\theta / \cos\theta\, u\phi$.[19] The locus of these velocity components trace out "pseudo" streamlines. On the unperturbed flow region (upper and right portion of the graph) the conical crossflow velocity converges to the origin of the coordinate system. The origin is on the y axis but at a distance of 0.3126 ft to the left of the corner at this location. The crossflow velocity components execute a sharp turn toward the corner at the shock wave generated by the wedge. On the wedge surface, a thin boundary layer is indicated. However, a strong flowfield development stands out just beneath the triple point as the crossflows with different orientation meet and accommodate each other. The emerging crossflow turns nearly or in excess of 180 deg with respect to the incoming stream. A strong vortex center is clearly reflected at a location immediately below the triple point.

The most striking features of the corner flowfield however, are indicated on the plate surface and in the vicinity of the corner. An orderly development of a boundary layer is noted from the outer edge of the plate. The pressure propagation from the embedded shock induces the flow separation which can easily be identified by the formation of the reverse flow. If one follows the trajectory of the vanishing crossflow velocity component, the trace leads to and terminates at the primary vortex center. This characteristic is totally different from two-dimensional flow separation. Again the observation is in agreement with Korkegi's conclusion in his study of three-dimensional flow separation for a corner configuration. The continuing growth of the reverse flow region as the flow proceeds downstream requires a continuous entrainment of fluid containing relatively low energy.

The crossflow enters the corner region beneath the triple point while retaining a relatively high level of the impact pressure and eventually impinges upon the wedge and the plate. This behavior was also observed in the experimental investigation, where Cooper and Hankey correctly identified it as an inviscid "finger."[12,19] After the crossflow negotiates the corner by reversing its orientation and moves outward

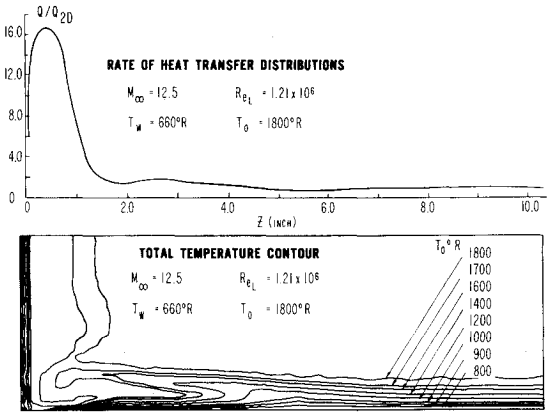

Fig. 12 Heat-transfer distribution and total temperature contour.

from the corner, a rapid expansion process occurs which is reflected in the surface pressure distribution (Fig. 2).

In Fig. 11, we present the contour plot of the crossflow Mach number based upon the magnitude of the conical crossflow velocity component. This graph defines the subsonic region of the flowfield. First, it substantiates the assertion made by Cooper and Hankey[12,19] that the flow region inboard of the triple point is subsonic, therefore negating the possibility of a pair of triple points as that of the symmetric corner. The inviscid finger is obvious, and the high-energy stream impinging and scavenging the surface also becomes evident. An extraordinary feature also emerges from the graph. Namely, a completely embedded supersonic crossflow region is created by the rapid expansion process mentioned earlier. The crossflow Mach number even reaches the maximum value of 1.56, (at the location 0.253 in. above the plate and 1.34 in. from the corner) which bears a close analogy to the imbedded supersonic region of a transonic airfoil. It is surmised that the existence of the supersonic region, followed by a compression shock, gives rise to the secondary vortex and associated second separation observed in the experiment.

In Fig. 12, the heat-transfer rate to the plate surface is presented together with a total temperature plot. The evidence of the inviscid finger and flow impingement on the solid surface is obvious. The high heat-transfer rate (by an order of magnitude) in the impingement areas on both the wedge and plate surface is in accordance with the understanding obtained from the analysis of the numerical results. Regretfully, there are no accompanying experimental data to facilitate a specific comparison for these exact flow conditions. However, the calculated heat-transfer rate on the plate closely resembles the experimental measurement under similar flow conditions.[25,26] Equally intense heat exchange on the wedge surface was also indicated by the present numerical solution.

Conclusion

A three-dimensional, time dependent Navier-Stokes code employing MacCormack's finite-difference scheme has been developed. Successful comparisons were performed for the three-dimensional compression corner flow at hypersonic Mach number and high Reynolds number laminar flow conditions. Agreement between the experimental data[12,19] and the numerical results was obtained for the surface pressure distributions, the impact pressure survey, and also the surface oil flow pattern. The prediction of a double-peak heat-transfer distribution on the plate surface is also in accordance with experimental observation.[25,26] This accomplishment demonstrated the feasibility to numerically investigate three-dimensional configurations. The methodology combined with a relatively general geometric package should be able to treat practical three-dimensional configurations encountered in engineering problems.

The present analysis verified the inviscid "finger," first identified by Cooper and Hankey in their investigation of the asymmetric corner configuration. In addition, the numerical results also revealed an imbedded crossflow supersonic region within the primary separation zone. Although the rather complex flowfield structure is a manifestation of strong viscous-inviscid interaction, the overall structure remains nearly conical.

Acknowledgment

The authors are indebted to D. S. McRae and D. D. Knight for their stimulating and fruitful discussions. We also appreciate the support provided by the NASA Ames Computational Fluid Dynamics Branch for use of the CDC 7600 computer for the high-resolution calculations.

References

[1] Stewartson, K., "Multistructured Boundary Layers on Flat Plates and Related Bodies," *Advances in Applied Mechanics*, Vol. 14, edited by Chia-Shun Yih, Academic Press, New York, 1974, pp. 146-234.

[2] Peyret, R. and Vivand, H., "Computation of Viscous Compressible Flows Based on the Navier-Stokes Equations," AGARDograph No. 212, Sept. 1975.

[3] Korkegi, R. H., "On the Structure of Three-Dimensional Shock Induced Separated Flow Regions," *AIAA Journal*, Vol. 14, May 1976, pp. 597-600.

[4] Kutler, P., "Numerical Solution for the Inviscid Supersonic Flow in the Corner Formed by Two Intersecting Wedges," AIAA Paper 73-675, Palm Springs, Calif., 1973.

[5] Shankar, V. and Anderson, D. A., "Numerical Solutions for Inviscid Supersonic Corner Flows," Engineering Research Institute, Iowa State Univ., Ames, Iowa, Final Rept. ISU-ERI-Ames-74090, May 1974.

[6] Weinberg, B. C. and Rubin, S. G., "Compressions Corner Flow," *Journal of Fluid Mechanics*, Vol. 56, Part 4, 1974, pp. 753-774.

[7] Ghia, K. N. and Davis, R. T., "A Study of Compressible Potential and Asymptotic Viscous Flows for Corner Regions," *AIAA Journal*, Vol. 12, 1974, pp. 355-359.

[8] Briley, W. R. and McDonald, H., "Solutions of the Three-Dimensional Compressible Navier-Stokes Equations by an Implicit Technique," *Lecture Notes in Physics*, Vol. 35, Springer-Verlag, Berlin, pp. 105-110.

[9] MacCormack, R. W. and Baldwin, B. S., "A Numerical Method for Solving the Navier-Stokes Equations with Application to Shock Boundary Layer Interactions," AIAA Paper 75-1, Jan. 1975.

[10] Shang, J. S. and Hankey, W. L., Jr., "Numerical Solutions for Supersonic Turbulent Flow over a Compression Ramp," *AIAA Journal*, Vol. 13, Oct. 1975, pp. 1368-1374.

[11] Shang, J. S., Hankey, W. L., Jr., and Law, C. H., "Numerical Simulation of Shock Wave-Turbulent Boundary Layer Interaction," *AIAA Journal*, Vol. 14, Oct. 1976, pp. 1451-1457.

[12] Cooper, J. R. and Hankey, W. L. Jr., "Flowfield Measurements in an Asymetric Axial Corner at $M=12.5$," *AIAA Journal*, Vol. 12, Oct. 1974, pp. 1353-1357.

[13] Crocco, L., "A Suggestion for the Numerical Solutions of the Navier-Stokes Equations," *AIAA Journal*, Vol. 10, Oct. 1965, pp. 1824-1832.

[14] Knight, D. D. and Hankey, W. L., Jr., "Numerical Simulations of Non-Chemically Reacting Radial Supersonic Diffusion Laser," AIAA Paper 76-60, Jan. 1976.

[15] MacCormack, R. W., "Numerical Solutions of the Interactions of a Shock Wave with a Laminar Boundary Layer," *Lecture Notes in Physics*, Vol. 8, Spring Verlag, 1971, p. 151.

[16] MacCormack, R. W. and Warming, R. F., "Survey of Computational Methods for Three-Dimensional Supersonic Inviscid Flows with Shock," *Lecture Series No. 64, Advances in Numerical Fluid Dynamics*, AGARD, 1973.

[17] Tannehill, J. C., Holst, T. L., and Rakich, J. V., "Numerical Computations of Two-Dimensional Viscous Blunt Body Flows with an Impinging Shock," *AIAA Journal*, Vol. 14, Feb. 1976, pp. 204-211.

[18] McRae, D. S., "A Numerical Study of Supersonic Viscous Cone Flow at High Angle of Attack," AIAA Paper 76-97, Jan. 1976.

[19] Cooper, J. R. and Hankey, W. L., Jr., "Flowfield Measurements in an Asymmetric Axial Corner at $M=12.5$," AIAA Paper 73-676,

Proceedings, AIAA 6th Fluid and Plasma Dynamics Conference, Palm Springs, Calif., Jan. 1973.

[20] "Theory of Laminar Flows," *High Speed Aerodynamics and Jet Propulsion*, Vol. IV, F. K. Moore (ed), Princeton University Press, 1964, pp. 387-390.

[21] Rosenhead, L., (Ed.), *Laminar Boundary Layers*, Oxford University Press, 1963, pp. 72-82 and pp. 488-490.

[22] Avduevskii, V. S. and Medvedev, K. K., "Separation of a Three-Dimensional Boundary Layer," *Fluid Dynamics*, Vol. 1, No. 2, 1966, pp. 11-15.

[23] Wang, K. C., "Separation of Three-Dimensional Flow," Martin Marietta Corp., MML TR-76-54C, Aug. 1976.

[24] Oskam, B., Vas, I. E., and Bogdonoff, "An Exploratory Study of a Three-Dimensional Shock Wave Boundary Layer Interaction at Mach 3," *AGARD Conference Proceedings*, On Flow Separation, No. 168, May 1975.

[25] Watson, R. D. and Weinstein, L. M., "A Study of Hypersonic Corner Flow Interactions," *AIAA Journal*, Vol. 9, July 1972, pp. 1280-1286.

[26] Schullz, H. D. and Baker, R. C., "Pressure and Heat Transfer Measurements in Regions of Three-Dimensional Shockwave-Boundary Interactions," Lockheed Missiles & Space Co., Sunvale, Calif., LMSC-D157341, March 1972.